

JPL Document 1539478

***TECHNOLOGY DEVELOPMENT FOR
EXOPLANET MISSIONS***

*Technology Milestone White Paper
Vortex Coronagraph Technology*

Gene Serabyn, P.I.

John Krist, Dimitri Mawet, Dwight Moody and John Trauger

25 March 2016

National Aeronautics and Space Administration
Jet Propulsion Laboratory
California Institute of Technology
Pasadena, California
© 2012 copyright. All rights reserved



Approvals:

Released by


E-SIGNED by Eugene Serabyn
on 2016-05-25 03:26:23 GMT

Gene Serabyn
Principal Investigator

Date

Approved by


E-SIGNED by Nick Siegler
on 2016-06-01 17:13:34 GMT

Nick Siegler
Exoplanet Exploration Program Chief Technologist, JPL

Date


E-SIGNED by Doug Hudgins
on 2016-05-25 17:56:35 GMT

Douglas Hudgins
Exoplanet Exploration Program Scientist, NASA HQ

Date

Table of Contents

1. Objective.....	3
2. Introduction/Background	3
2.1. The Vortex Coronagraph.....	3
2.2. Vortex Phase Masks	5
2.3. Limitations of Optical Vortex Phase Masks	10
2.4. Broadband Optical Vortex Coronagraphs.....	10
3. Milestone Definition	15
3.1. Relevance for a Future Exoplanet Mission	16
4. Experiment Description	17
4.1. The Compact Coronagraph	17
4.2. Differences Between Flight and Laboratory Demonstrations	19
5. Data Measurement and Analysis	20
5.1. Definitions	21
5.2. Measurement of the Star Brightness	22
5.3. Measurement of the Coronagraph Dark Hole Contrast Field	23
5.4. Milestone Demonstration Procedure	23
5.5. Milestone Data Package	24
6. Success Criteria	24
7. Schedule.....	25
8. References	26

TDEM Milestone White Paper: Vortex Coronagraph Technology

1. Objective

In support of NASA’s Exoplanet Exploration Program and the ROSES Technology Development for Exoplanet Missions (TDEM), this whitepaper explains the purpose of the first TDEM Milestone for the project entitled *Broadband Light Rejection with the Optical Vortex Coronagraph*, specifies the methodology for computing the milestone metrics, and establishes the success criteria against which the milestone will be evaluated. The milestone is concerned with the demonstration of high rejection of broadband (10 – 20% bandwidth) light, so as to attain performance levels required by space missions.

2. Introduction/Background

2.1. The Vortex Coronagraph

The ideal optical vortex coronagraph operates as follows (Mawet et al. 2005; Swarzlander 2009, Serabyn & Mawet 2012). An unobstructed telescope’s input pupil can be described by a field distribution, $P(r)$, of

$$P(r) = \begin{cases} 1 & \text{for } r < A \\ 0 & \text{for } r > A, \end{cases} \quad (1)$$

where r is the radial coordinate, and A is the radius of the input aperture. Focusing the light leads, via the usual Fourier transform relation between focal and pupil planes, to the normal Airy-function focal-plane field distribution,

$$E_f(\theta) \propto \frac{J_1(kA\theta)}{kA\theta}, \quad (2)$$

where J_1 is the Bessel function of order 1, k is the wavenumber, and θ is the angular radial offset from the center of the stellar PSF.

Centering a transmissive optical vortex phase mask on this focal-plane electric field distribution multiplies the field by a phase factor corresponding to an azimuthal phase ramp, i.e., $e^{in\alpha}$, where α is the azimuthal angle, and n is the “topological charge” of the vortex (the number of 2π ’s of phase that one circuit about the center provides), yielding

$$E_f(\theta, \alpha) \propto e^{in\alpha} \frac{J_1(kA\theta)}{kA\theta}. \quad (3)$$

After passage through the vortex phase mask, the light is recollimated by, e.g., an off-axis paraboloid, yielding a downstream image of the pupil. Because of the applied azimuthal phase and the definition of $J_n(x)$, the Bessel functions of order n , that being

$$J_n(x) = \int_{-\pi}^{\pi} e^{-i(n\alpha - x\sin(\alpha))} d\alpha, \quad (4)$$

the downstream pupil plane distribution for, e.g., a charge 2 vortex is proportional to (Mawet et al. 2005; Swartzlander 2009; Serabyn & Mawet 2012)

$$\int_0^\infty J_2(kr\alpha)J_1(kA\alpha)d\alpha \quad (5)$$

instead of the usual

$$\int_0^\infty J_0(kr\alpha)J_1(kA\alpha)d\alpha. \quad (6)$$

This change in the integrand has the effect of altering the resultant pupil distribution dramatically, moving all of the light, which originated entirely inside the entrance pupil, to the exterior of the pupil. In the ideal case, a uniformly zero field remains inside the pupil (see Fig. 1, top right panel, for the charge 2 case). In the general case of an arbitrary (but even) topological charge, the post-vortex pupil plane field falls off from the pupil rim as r^{-n} , with still a zero field inside. As a result, the starlight can be completely blocked by a simple opaque stop (i.e., a circular hole) in the downstream pupil plane that is matched to the pupil radius. Of course with wavefront aberrations present, residual light will appear inside the pupil, which will need to be minimized with wavefront control.

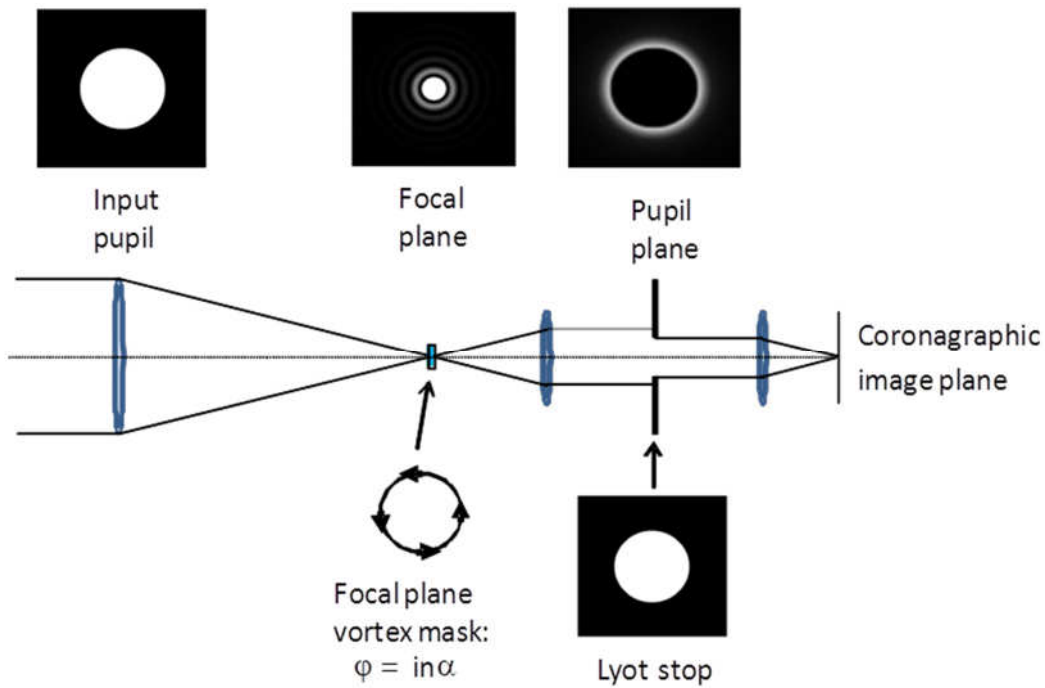


Figure 1. Layout of the optical vortex coronagraph: an optical vortex phase mask in the focal plane yields a downstream pupil image in which all of the on-axis starlight appears outside of the original pupil's image, where it is blocked by an aperture (Lyot) stop.

2.2. Vortex Phase Masks

This TDEM project aims at the high-contrast testing of optical vortex phase masks in the compact coronagraph (CC) testbed. The testbed is discussed in Section 4; here we first discuss the vortex phase masks. Several different manufacturing approaches to making vortex masks exist, as discussed in, e.g., Mawet et al. (2011a). Simply put, our ultimate goal is to reach broadband high contrast with *any* vortex phase mask, regardless of the specific type of vortex mask. However, based on past experience and current manufacturing capabilities, our baseline plan is to develop and test vector vortex phase masks made of liquid crystal polymer (LCP) layers. A vector vortex phase mask is a spatially variant half-wave plate (HWP) structure in which the optical-axis orientation pattern is used to change the phase of the beam as a function of lateral position (Fig. 2). Since a vector vortex mask is a HWP structure, at each point an input circular polarization state is reversed, but the output phase is set by the local orientation of the fast axis. Thus, with a properly selected optical axis orientation pattern (e.g., Fig. 2), the output phases can be set to match the desired azimuthal phase ramp.

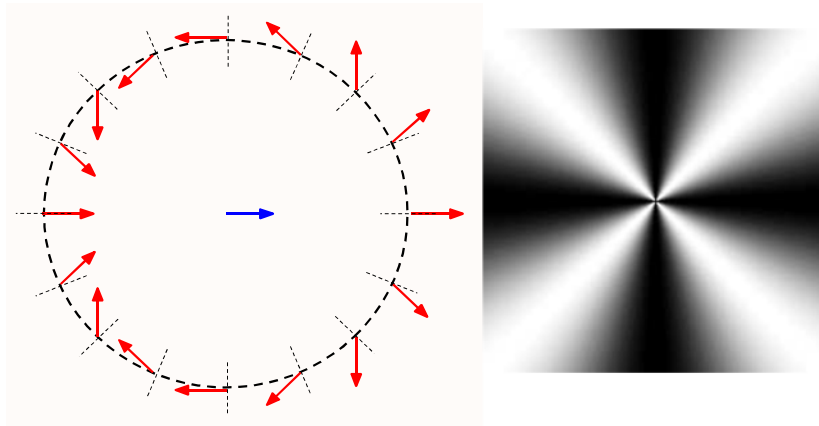


Figure 2. *Left: The optical axis orientations (dashed lines) in a second-order liquid crystal polymer vector vortex phase mask. The structure is a spatially-variant half-wave plate (HWP) with a radial optical axis orientation, i.e., the optical axis rotates about the center in sync with the azimuthal coordinate. The effect of such a HWP on a linear input polarization (blue arrow) impinging on it (selected by an upstream horizontal linear polarizer here) is to rotate the output polarization by twice the angle between the incident polarization direction and the optical axis. The output linear polarization thus rotates as twice the azimuthal angle (red arrows). If the input vector is now imagined to be spinning (in a circular polarization state), all of the output red vectors spin as well, but each has a different orientation at any given fixed starting time (as shown). The increasing initial angles (at a fixed time) in a path around the center correspond to the desired azimuthal phase gradient characteristic of a vortex beam. Right: computation of the periodic modulation of the intensity transmitted by an OVVC between crossed polarizers. Now imagine following the horizontal linear polarizer and vortex phase mask with a vertical linear polarizer. Examination of the directions of the red arrows in the figure on the left shows that transmission maxima will occur at $\pm 45^\circ$, with minima at 0° and 90° .*

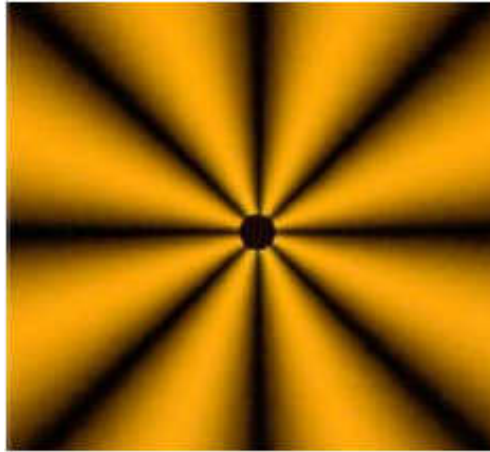


Figure 3. A real fourth-order liquid crystal polymer vortex phase mask manufactured by JDS Uniphase, measured between crossed polarizers on a polarizing microscope. In a fourth order mask, the output phase spins twice as fast in a circular path about the center as in a second order mask, yielding 4 dark stripes instead of two. Moreover, in this actual device, a central defect occurs in the vortex pattern near the central singularity, which is masked off by an opaque metal spot.

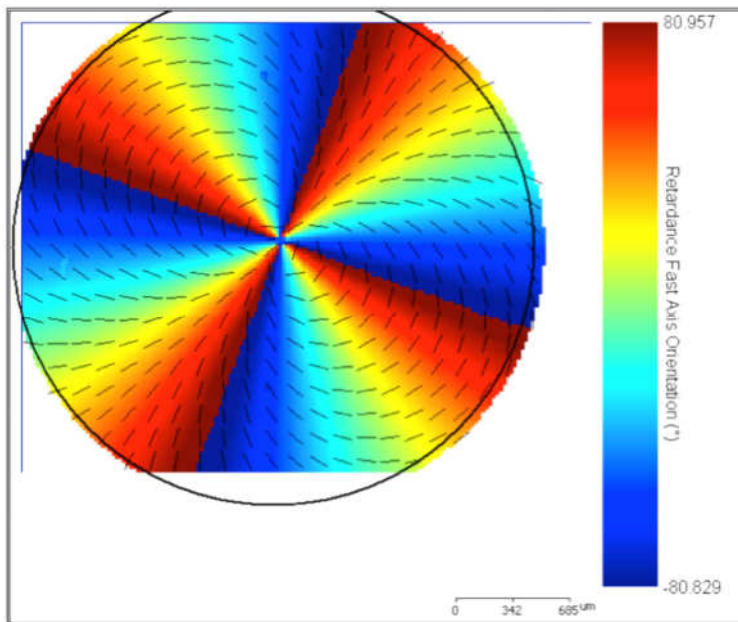


Figure 4. The optical axis orientation map of a fourth-order liquid crystal polymer vortex phase mask that was manufactured by Beam Engineering, as measured on a Muller matrix imaging polarimeter at JPL. Here the optical axis orientation (shown by the little lines and in color) spins twice as fast as the azimuth in a circular path about the center.

We obtain our vortex masks from a number of commercial vendors. Initial characterization and vetting of our vortex masks prior to high-contrast CC testing will be carried out with standard optical instruments available at JPL such as a polarizing microscope, which shows a vortex mask transmission through crossed linear polarizers (e.g., Figure 3), and a Mueller matrix imaging polarimeter, which gives both optical axis orientations (e.g., Figure 4) and retardance (phase delay).

Beyond our baseline plan of LCP masks, we may also have access to photonic crystal vortex phase masks produced by our Japanese colleagues (Murakami et al. 2014). As usually only a couple of days are needed to reveal the high contrast capabilities of a given mask, it will be possible to fit brief CC tests of such alternate-technology masks into our schedule, should promising masks become available. Indeed, such tests may be very useful as a comparison diagnostic for the CC, potentially aiding in the discrimination between different light leakage origins. However, to be clear, no other potential mask types are in our baseline plan; they are viewed purely as a potential bonus.

Our prior baseline monochromatic LCP mask design, as developed in concert with JDS Uniphase, is shown in cross-section in Figure 5 (Mawet et al. 2009). During our earlier TDEM award, such a mask was used to reach a single-polarization, monochromatic contrast of 5×10^{-10} over a region defined (Figure 6) by a cut-off hemisphere between 3 and $8 \lambda/D$ (Serabyn et al. 2014). Our previous monochromatic milestone results are shown in Figs. 7 and 8.

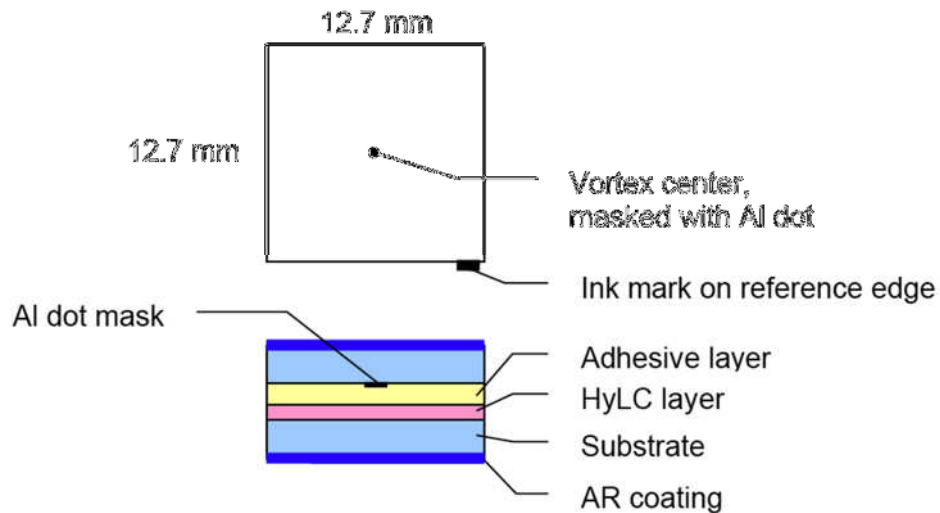


Figure 5. Cross-section of the sandwich design of our current monochromatic LCP vortex masks. The hybrid LCP (HyLC) layer is deposited on one substrate and a small opaque dot mask is placed upon another substrate, and the two are then glued together, with the dot centered over the vortex.

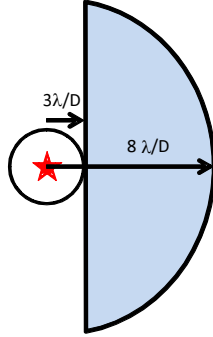


Figure 6. Target high-contrast dark field for both our previous TDEM and this one. As described in the text, inner and outer regions are defined for a one-sided dark field. The location of the suppressed central star is indicated in red. The target dark hole for this demonstration would also be from 3 to $8\lambda/D$, as defined in this figure.

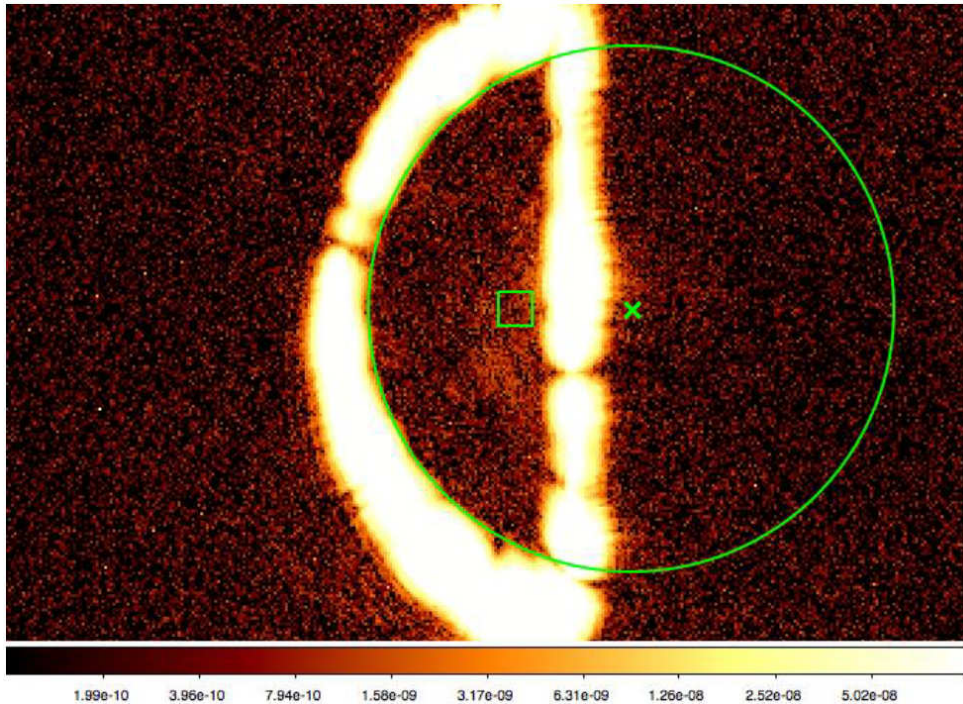


Figure 7. Final monochromatic dark hole (the interior of the reverse-D-shaped region) obtained at the end of the first milestone run of our previous TDEM project. The average contrast (with contrast being the calibrated ratio of the dark hole pixel value to the value of the brightest pixel in the unattenuated star image; see Section 5) in this dark hole is 4.1×10^{-10} . The green “guides” are an $8\lambda/D$ radius circle, a $3-4\lambda/D$ square, and a cross marking the “star” location.

Our earlier prime manufacturer of LCP vortex phase masks, JDS Uniphase, has recently informed us that they have decided to leave the field of vortex phase mask manufacture. We have thus recently been working with two different vendors of LCP vortex masks, those being Beam Engineering and ImagineOptics/NC-State. Luckily, it turns out that the technologies available to both of those entities are more suited to making broadband masks anyway (twisted layers; see below), so this change in vendors may have been inevitable anyway.

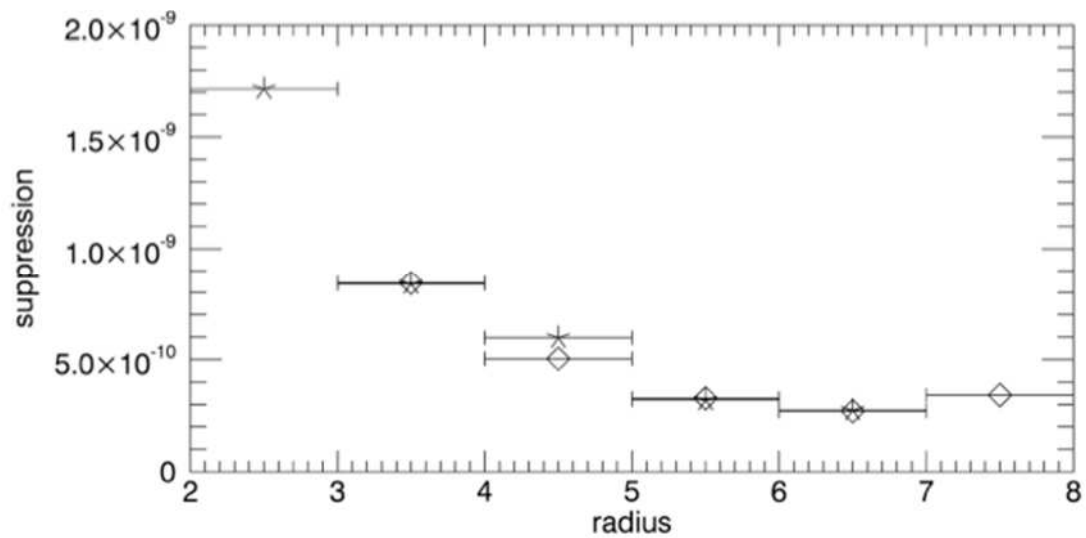


Figure 8. Radial contrast curves for a vortex phase mask in the HCIT, measured across dark holes extending from 3 to 8 λ/D (diamonds), and 2 to 7 λ/D (stars).

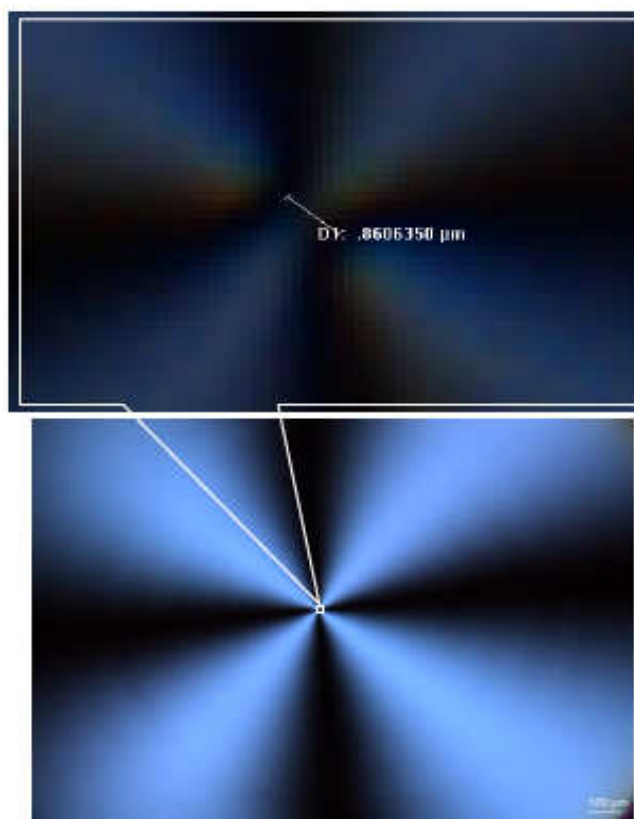


Figure 9. A recent vortex phase mask manufactured by Beam Engineering with an ~ 1 micron-sized central defect. No central covering was applied.

2.3 Limitations of Optical Vortex Phase Masks

As discussed in Mawet et al. (2011a) and Serabyn & Mawet (2012), limitations to the coronagraphic rejection provided by vector vortex phase masks arise in several ways, including imperfections both in the phase masks themselves and in the focal plane diffraction pattern coupled to the mask, the latter of which can be addressed by active wavefront correction. Mask imperfections can arise in deviations from the desired half-wave retardance, which is nominally met only at a number of design wavelengths, in deviations of the optical axis orientations from the desired pattern, which tends to be a problem near the center of the vortex, in extra (ghost) reflections from the optical interfaces within the vortex’s layered structure, and in material irregularities, which serve as scattering centers. Previous work has lowered the size of the defect at the center of LCP vortex phase masks to the micron scale (Fig. 9), and in any case, the residual central defect can be covered with a small central blocker (Fig. 10) if the central defect is unacceptably large. Likewise, extra ghost reflections can be reduced to acceptable levels through index matching. Our focus in this TDEM is thus the main residual issue – increasing the bandwidth of vortex phase masks

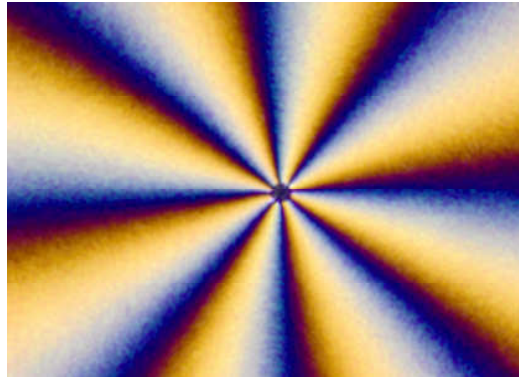


Figure 10. *The central region of a charge 4 optical vortex phase mask manufactured by NC State, with a 6-8 micron diameter opaque covering on the central vortex defect.*

2.4 Broadband Optical Vortex Coronagraphs

To be useful for exoplanet observations, a coronagraph must reject starlight over a broad bandwidth. However, for the simplest half-wave plate structures, the half-wave condition is usually satisfied only at a single design wavelength, λ_0 . For wavelength-independent indices of refraction, the stellar leakage will then depend on wavelength, λ , as

$$I_L/I_{in} = (\pi/2)^2 ((\lambda-\lambda_0)/\lambda_0)^2. \quad (1)$$

The off-center-wavelength stellar leakage will appear in the post-vortex pupil plane as a uniformly illuminated pupil with the light in the initial circular polarization state (as opposed to the bulk of the post-vortex starlight, which flips its circular polarization state and ends up outside of the geometric pupil). The spectral leakage thus results in a focal-

plane Airy pattern in the original polarization state. Integrating a flat spectrum source over a passband of width $\Delta\lambda$ then gives a total leakage of

$$L = (\pi^2/48) (\Delta\lambda/\lambda_0)^2. \quad (2)$$

For example, a 10% bandwidth will have a total stellar leakage of $\approx 2 \times 10^{-3}$. The leakage will fall with off-axis distance as an Airy pattern, and at $2\lambda/D$, the leakage will be at approximately the 10^{-5} level. For deeper contrasts, a means of suppressing broadband radiation is thus needed. Two techniques for passband broadening are possible: multi-layer half-wave designs that yield more intrinsically broadband vortex masks, and spectral broadening of a mask's intrinsic rejection by means of polarization filtering. We plan to employ both of these approaches, and now describe each of them in turn.

As described earlier, a vector vortex is a geometrical structure, i.e., a spatially variant HWP in which the optical axis orientation is a function of position. A vector vortex is thus achromatic to first order by virtue of the geometry of its structure. For perfect HWP phases, this geometric structure flips the input circular polarization state, and sends that light outside of the pupil. However, the retardance, which ideally is 180° , is actually a function of wavelength. Wavelength-dependant deviations from the ideal retardance of 180° thus allow light to leak through in the original circular polarization state, and this light remains within the pupil [19]. Thus, one way of obtaining more broadband performance is to use polarization filtering to reduce the spectral leakage, i.e. to reject the residual starlight in the original circular polarization state (Fig. 11) which is inside the pupil. Of course this involves splitting the two polarization states upstream of the vortex. This approach thus relies on the combination of a Lyot stop to remove the bulk of the direct starlight outside the pupil, and polarization filtering to remove the chromatic leakage inside the pupil.

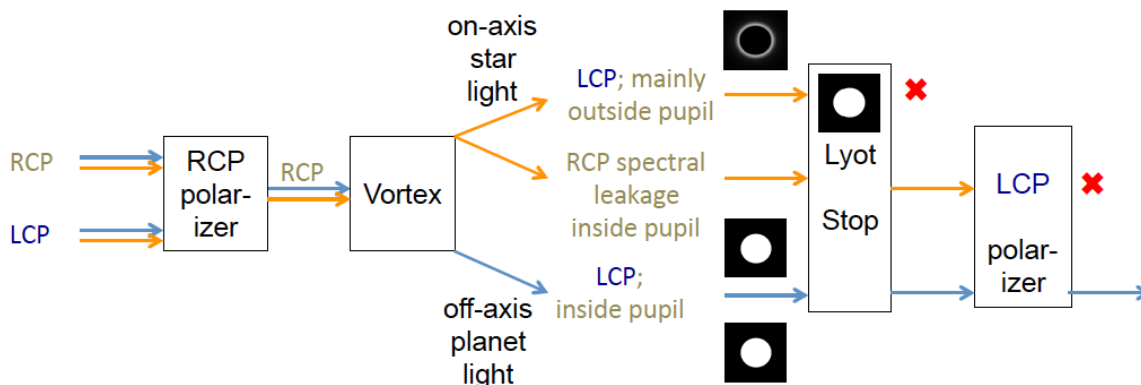


Figure 11. Spectral polarization filtering. The starlight is shown in orange, and the planet light in blue. RCP and LCP stand for right circular polarization and left circular polarization, respectively. The starlight outside the pupil is rejected by a Lyot stop (aperture), while the spectral starlight leakage inside the pupil is rejected by a circular polarizer.

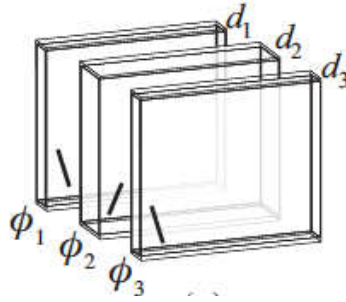


Figure 12. *Classical uniform multilayer approach to broadening waveplate passbands (Komanduri et al. 2032). The successive optical axis orientations are shown.*

The second solution to achromatizing a vortex phase mask is to use an achromatized HWP design. Many approaches are conceivable (e.g., Kommanduri et al. 2013), and of these, the conceptually simplest approach would be to use the well-known technique for achromatizing waveplates [24] using multiple fixed half-wave layers. A three-layer design is fairly straightforward: the three layers are all identical, but with axes rotated with respect to each other by angles of, e.g., $\sim 0^\circ$, 60° , and 0° (Fig. 12). A one-layer design yields ~ 0.1 radian rms retardance error over a 20% bandpass, while three layers would in theory reach the 0.001 radian rms level. Since contrast is proportional to rms^2 , with three layers one can reach 10^{-9} - 10^{-8} off-axis contrasts (beyond $2 \lambda/D$) over a significant band, while a 5-layer device would exceed the needs of exoplanet missions.

However, our earlier initial attempt at a three-layer HWP vortex using LCP layers with vertically-uniform layer orientations had limited success, both because sharp discontinuities in molecular/optical-axis orientations in adjacent LCP layers lead to directional distortions near the layer boundaries, and because it proved difficult to align the centers of the successive layers accurately.

There is however a more promising approach - the use of “twisted” LCP layers, in which the orientation within each layer rotates smoothly as one progresses vertically through the layer, reaching at the end of one layer the exact boundary orientation required at the start of the next layer (Fig. 13). Boundary discontinuities are thus eliminated, as the previous layer correctly initiates orientation of the next layer. Note that this also includes the location of the center of the vortex, thus obviating both problems at once. Both of our current vendors have experience with this approach; indeed one of them invented it (Komanduri et al. 2012). Figs. 14 and 15 show some initial results already obtained with broadband vortex masks manufactured with the twisted multi-layer approach by both potential vendors. Evidently this approach does yield increased bandwidths in practice; the goal now is thus to lower the errors into the acceptable range, and to test these masks in a very high contrast coronagraph such as the CC to establish what they (and their successors) can do in practice.

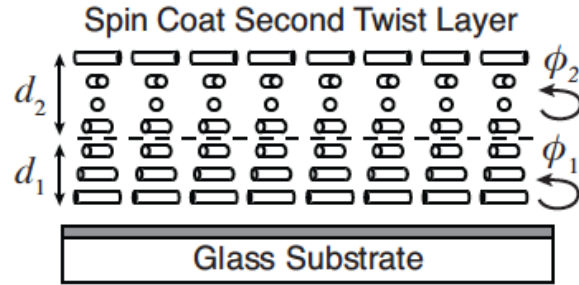


Figure 13. Internal rotation of LCP layers (Komanduri et al. 2012)

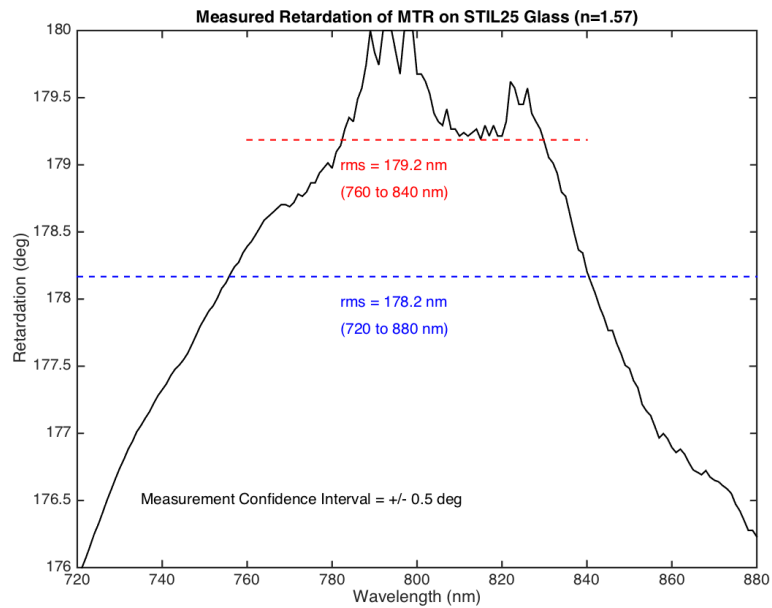


Figure 14. Retardation vs. wavelength for a NC State optical vortex centered at a wavelength of 800 nm. Two twisted layers were used. This mask deviates by 0.8° rms (0.014 rad) over a 10% passband. (Note that the labeling in the figure should read 179.2° and 178.2° , not nm).

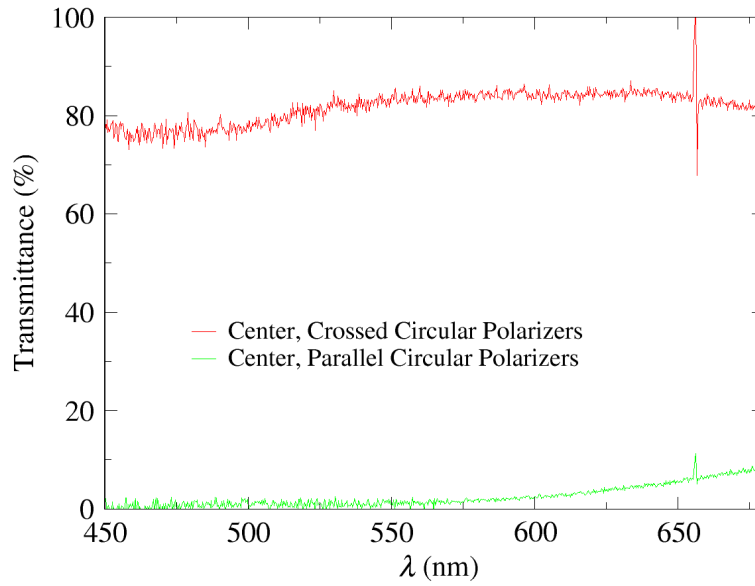


Figure 15. *Green curve: Transmission through parallel circular polarizers of a Beamco broadband twisted-multi-layer optical vortex mask. The low transmission region from 450 to 550 nm (corresponding to high rejection by the vortex) covers close to 100 nm, or ~ 20% bandwidth.*

3. Milestone Definition

TDEM Technology Milestones are intended to document progress in the development of key technologies for a space-based mission that would detect and characterize exoplanets, such as Exo-C, Habex and LUVOIR, thereby gauging the mission concept's readiness to proceed from pre-Phase A to Phase A. This milestone addresses broadband starlight suppression with the optical vortex coronagraph, and its objective is the validation of the vortex focal plane mask with broadband light. This milestone thus focuses on the validation of one key TDEM technology – the vortex mask. Success is defined in terms of quantified performance demonstrations of this key technology, ideally with minimal sensitivity or dependence on extraneous environmental factors.

Milestone 1: Broadband Starlight Suppression with Optical Vortex Phase Masks

Using optical vortex phase masks, demonstrate a calibrated average coronagraph contrast of 1×10^{-9} or better over angular separations of $3 \lambda/D$ to $8 \lambda/D$ from the input point source, for any 10% bandwidth in the wavelength range 300 –1000 nm, for at least one polarization state.

The “angular separations” are defined in terms of the wavelength λ and the diameter D of the aperture stop on the deformable mirror (DM), which is the pupil-defining element of the laboratory coronagraph. For this milestone, the pupil stop at the deformable mirror (DM) must be at least 16 mm diameter, the absolute minimum required for a dark hole to be able to reach out to $8 \lambda/D$ for 1 mm actuator spacing.

As stated in the milestone, our performance metric is the average contrast in the specified dark hole region. Contrast is defined for any point in the field as the calibrated ratio of the residual light level at that location to the light level at the peak pixel of the point source point spread function in the absence of a coronagraphic mask.

3.1. Relevance for a Future Exoplanet Mission

Development of vortex technology is intended to advance the readiness of mission concepts for the coronagraphic imaging and spectroscopy of exoplanetary systems. The small inner working angle (IWA) capability of the vortex coronagraph allows consideration of a range of mission sizes, from probe-scale (Exo-C) to many meter diameter flagship-scale missions (Habex and LUVOIR). Exoplanets in the super-Earth to Jovian range occur at contrasts of $\approx 10^{-9}$, motivating our milestone demonstration level. Post-processing techniques (not addressed here) may be able to improve contrast further by roughly an order of magnitude (Trauger and Traub 2007).

Exoplanet imaging missions form a high contrast “dark hole” or “dark field” over a working angle spanning $\sim n_i\lambda/D$ to $n_o\lambda/2D$, where n_i sets the IWA, as defined by the science requirements, the intrinsic capabilities of the coronagraph, and the wavefront and pointing control capabilities of the mission, and n_o sets the outer working angle (OWA). In general, n_o is somewhat smaller than n_{DM} , the number of actuators across the deformable mirror, to allow for realistic (i.e., finite) gradients in the transition from the dark hole region to the light region beyond the outer edge of the dark hole.

An IWA of $4\lambda/D$ was set by the TPF-C science requirements in the TPF-C STDT report (Levine et al. 2006), and WFIRST plans to use an IWA of $3\lambda/D$. Somewhat smaller IWA values are theoretically possible with the vortex coronagraph, but as our goal here is to address bandwidth performance issues, we set our milestone IWA at $3\lambda/D$ as well, to agree with both our earlier monochromatic vortex milestone, and with the WFIRST requirements. However, we do plan to keep an unofficial goal of moving to even smaller angles, as we successfully did with our earlier monochromatic TDEM.

The OWA ($< n_{DM}\lambda/2D$) is defined by the highest spatial frequency controlled by the deformable mirror (DM) aperture used. The CC DM has 1024 actuators controlling the surface of a 32×32 mm mirror facesheet, so our largest conceivable OWA, allowing again for a finite ($2\lambda/D$ wide) transition from dark to light, would be of order $14\lambda/D$ (since the actuators are spaced by 1 mm). However, we will not employ this maximum conceivable OWA, for several reasons. First, we wish to be able to employ off-the-shelf 1-inch-diameter polarization and waveplate components, which, removing 2 mm of radius for vignetting by retaining rings, would limit our collimated beam to a radius of roughly 10.5 mm. (Note that polarization components will allow for some discrimination between error budget terms, and a single-polarization vortex coronagraph may in any case be required for reaching very high contrast.) Allowing again for a $2\lambda/D$ transition width from dark to light, this then leaves us with a maximum dark hole outer radius of $8.5\lambda/D$. Second, extensive optical modeling and tolerancing has shown that it becomes increasingly difficult to control the contrast in the dark field as one moves closer to the image of the target star, so, for a fixed dark-hole contrast goal, a smaller OWA makes a fixed target contrast *more difficult* to achieve, as outer even darker regions are excluded from the dark hole. Our milestone is thus aimed at the most challenging inner region of the image plane. Finally, our selected OWA is also sufficiently large that the physics of the wavefront control problem can be demonstrated with high expectation of applying the same approach to a larger dark field at a later date. For all these reasons, we use an OWA of $8\lambda/D$.

4. Experiment Description

4.1. The Compact Coronagraph

Our vortex phase masks will be tested in a new testbed facility at JPL, called the compact coronagraph (CC) herein. The current layout and the parameters of the CC's optical table are shown in Figure 16. The optical system resides in a vacuum chamber (Figure 17) that can be evacuated to ~ 10 milliTorr. This configuration will be modified by the addition of two circular polarizers (each composed of the combination of a linear polarizer and a quarter-wave retarder), the first inside the light source assembly, S, to generate a single pure circular polarization state, and the second just after the Lyot stop (roughly at the "pivot -90° " location). (The two "pivot" labels carry no meaning and can be ignored.)

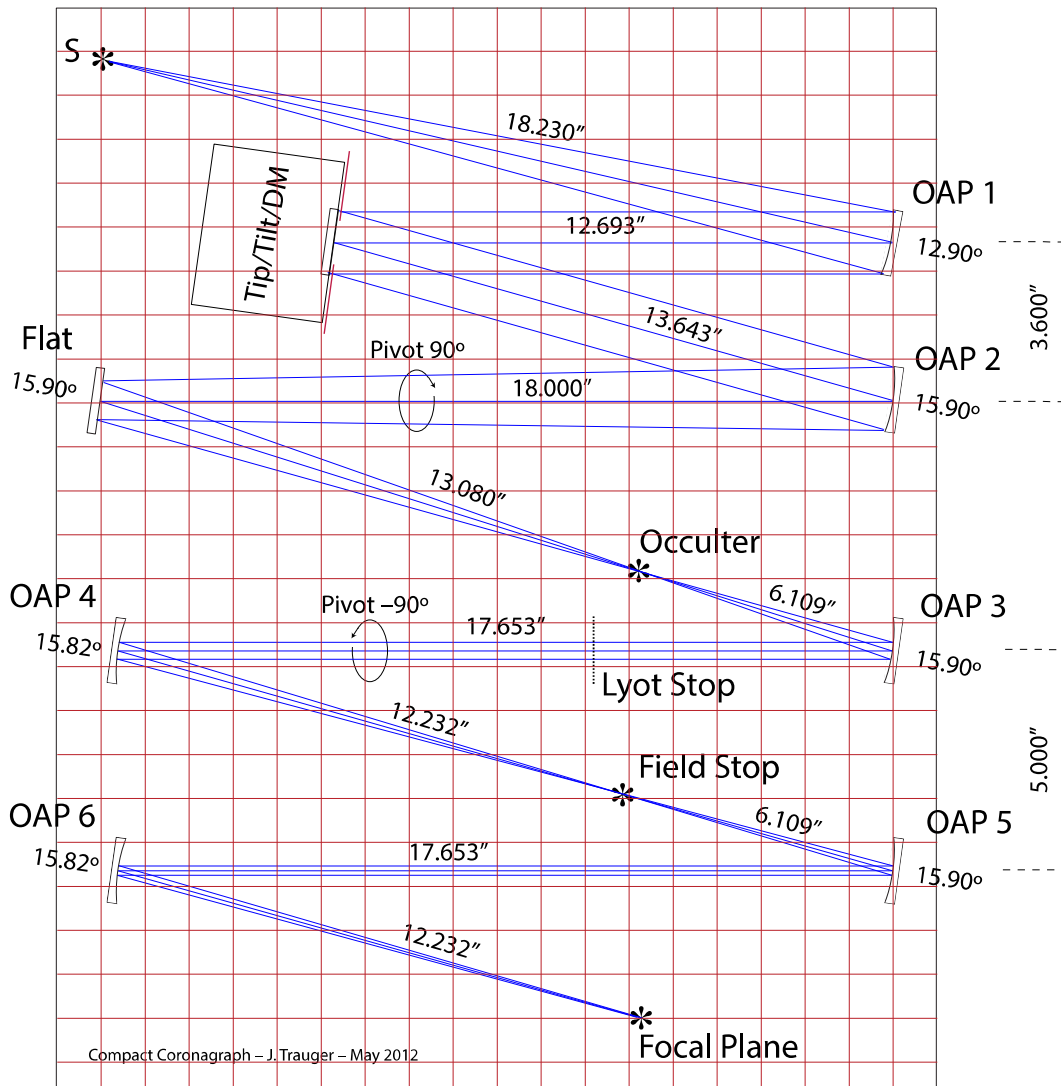


Figure 16. Optical layout of the CC coronagraph bench. The optical elements in the optical path starting from the source, S, are as follows. The light source (which is planned

to contain an internal polarizer and quarter wave plate to select one input circular polarization state) illuminates OAP1, the first of six off-axis paraboloidal (OAP) mirrors, where the beam is collimated. The beam passes to the combined tip/tilt/deformable mirror (DM), where an aperture stop defines the pupil of the system. The DM is from Xinetics, with 1024 actuators driving a mirror facesheet measuring 32×32 mm. The collimated light is then focused by OAP2 and folded by a flat mirror, passing to the focal plane where the vortex mask will be located (the “occulter” location). The beam is then collimated by OAP3 on its way to the Lyot stop, which is located in a pupil plane conjugate to the deformable mirror. A quarter-wave plate and polarizer can be placed just after the Lyot stop to select one output circular polarization state. The collimated beam is then brought to a focus by OAP4 to create the high-contrast coronagraph image. A camera, formed by a pair of small OAPs, then magnifies and projects the coronagraph image onto the CCD focal plane. Polarizers and quarter wave plates will be inserted in two locations, as described in the text.

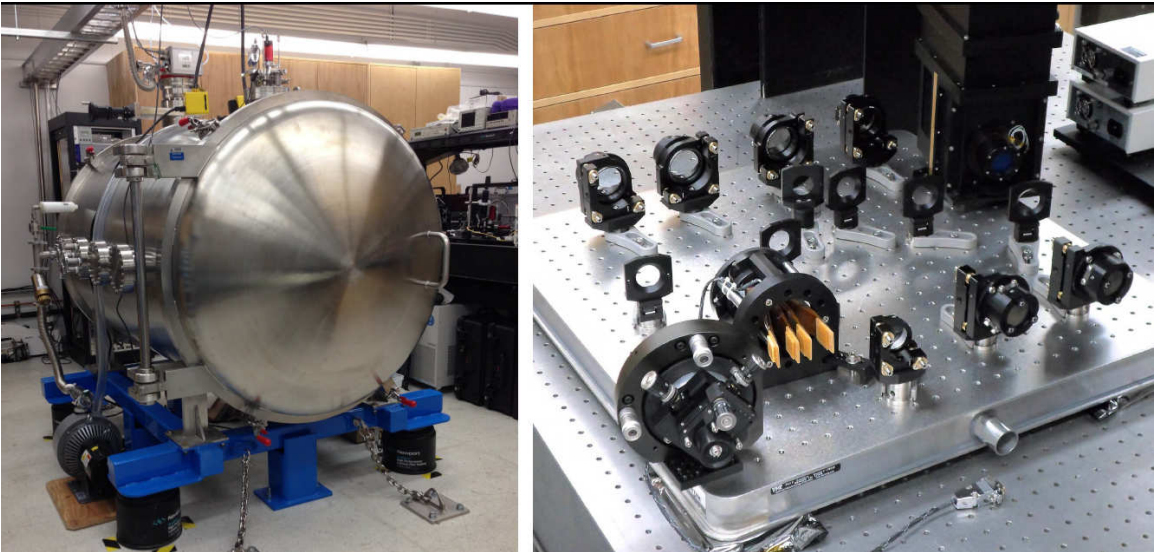


Figure 17. Left: The compact coronagraph vacuum chamber. Right: The compact coronagraph optical bench.

The milestone demonstration will rely on a wavefront sensing and correction process that has been used in previous high-contrast demonstrations, including our earlier HCIT vortex demonstration. A variant of the “electric field conjugation method” (EFC), as described in Give’on et al. (2007), is used and iterated as necessary. For a given wavelength, and starting with a nominally flat surface figure setting on the DM, we will: (a) take a set of contrast field images with the initial DM setting; (b) take images for each of four “probe” DM settings (consisting of small deterministic surface figure deviations from the initial DM setting), (c) use these data to compute the complex electric field in the target dark field region; and then (d) calculate and apply a new DM setting that will reduce the energy over the dark field, thus establishing a new “initial DM setting” in preparation for the next iteration, which is a loop back to step (a). A typical integration time for an individual image is expected to be about 10 sec, and one complete wavefront sensing and control

cycle, including overhead for CCD readouts, data handling and computations, is expected to take ~ 10 minutes.

4.2. Differences Between Flight and Laboratory Demonstrations

There are several differences between the lab demonstration and flight implementation.

Starlight: In a space coronagraph, the spectrum of light illuminating the coronagraph would closely resemble black body radiation. For this first milestone, the source will be a broadband supercontinuum source with selectable optical filters of various bandwidths and passbands. This source provides a photon flux that is comparable to or somewhat brighter than the target stars to be observed. The goal of this milestone is to demonstrate the contrast that can be achieved, independent of the source intensity. A bright source is a convenience that does not compromise the integrity of the demonstration, as it affects only the integration times.

Unlike the light collected by a telescope from a target star, the light intensity is not uniform across the pupil. Typically this non-uniformity is a center-to-edge “droop” of a few percent corresponding to the diffraction pattern from a small pinhole. This small level of non-uniformity is expected to have negligible effect on the final contrast if it is accounted for in the wavefront control algorithm, and is expected to result in a finite but below-requirement loss of contrast if it were ignored in the control algorithm.

Spacecraft dynamics: A control system is required in flight to stabilize the light path against motions of the spacecraft. The dominant effects of spacecraft dynamics are jitter of the star image on the coronagraphic focal plane mask and beam walk in the optics upstream of the focal plane mask. For a specific example, the ACCESS analysis showed that for fourth-order coronagraphs (including Lyot, vortex, and pupil mapping coronagraphs) with an inner working angle of $3\lambda/D$, rms pointing errors need to be $< \pm 0.03 \lambda/D$ to limit the contrast degradation to $< 2 \times 10^{-10}$. The concept models have shown that the required pointing stability can be achieved in space with current high Technology Readiness Level (TRL) systems. Scaled to the CC, this would correspond to an ability to center the vortex mask on the “star” within about $2.5 \mu\text{m}$, or about 0.2 pixel when projected to the CCD focal plane.

The milestone demonstration requires passive stability of the testbed, which is thus untraceable to spacecraft dynamics. In practice, the CC may exhibit alignment drifts that are larger than expected in the space environment. If so, we will rely on favorable periods of thermal and mechanical stability of the CC.

Single deformable mirror: The milestone demonstrations will be carried out with a single DM, which allows the control of phase and amplitude in the complex wavefront over one half of the coronagraph field described. In flight, for some missions, a pair of DMs may be used in series to generate a full two-sided dark hole, with the added advantages of a deeper contrast field and better broadband control.

On the other hand, with the exception of the second DM, and the actual size of the DM, the layout of the vortex coronagraph in the HCIT is essentially the same as is being

proposed for space missions (Exo-C, WFIRST, Habex, LUVOIR). The layout will also allow us to probe the need to separate polarization states to reach high contrast.

5. Data Measurement and Analysis

In brief, a contrast measurement is a measurement of the intensity of the residual light (speckles, background, etc.) within the dark field, relative to the peak intensity of an image of the source. There will of course be a distribution of intensities across the dark hole, from which the average contrast and its statistical confidence level will be calculated. The milestone objective is to demonstrate with high confidence ($\geq 90\%$) that the true contrast in the dark field, as estimated from our measurements in the presence of noise, is equal to or better than the required threshold contrast, $c_0 = 1.0 \times 10^{-9}$.

Because of laboratory instabilities and the ongoing wavefront control algorithm, the contrast at any point in the dark field is time dependent, and so multiple successive exposures of the dark hole will be taken. For each image (where “each image” can itself be more than one sequential image if temporal averaging is deemed important to build up signal to noise), we calculate a spatial average of the measured contrast level over the entire dark hole. This yields a series of n (with n required to be ≥ 4) individual dark hole images, each with its own spatially-averaged dark hole contrast, c_i . We next take an average over the series of n dark hole images, leading to a sample-averaged contrast and variance, both defined below. To avoid confusion, we refer to spatial averages over an image region as “averages”, and averages of quantities over a number (sample) of images as “means”. Finally, we note that the entire experimental run is then to be repeated from scratch at least 3 times, to show repeatability. No averaging is done over the independent runs, so that the milestone is achieved independently m times.

As mentioned, the measured contrast is time dependent, being subject to laboratory conditions such as the quality of the optical components, their alignment, drifts in their alignment over time, and the effectiveness of each wavefront sensing and control cycle. With each iteration, our nulling procedure attempts to improve the contrast, thus compensating for any drift or alignment changes that may have occurred since the previous iteration. Further variations may be expected due to experimental noise and any limitations in the algorithm. The images built up from a sequence of such iterations will provide a distribution of contrast values, which will be regarded as Gaussian about a mean contrast for the data set. We therefore consider the mean contrast value as representative of the true contrast value for a given data set.

The contrast measurements of the iterations within a single run will fluctuate due to a both random wavefront control errors and random measurement errors. The statistical confidence level will thus require an estimation of the variance. Given that our speckle fields contain a mix of static and quasi-static speckles (the residual light field remaining after the completion of a wavefront sensing and control cycle, together with the effects of alignment drift following the control cycle), as well as other sources of measurement noise including photon detection statistics and CCD read noise, an analytical development of speckle statistics is impractical. We will thus to compute the confidence coefficients on

the assumption of Gaussian statistics. The full set of measurement will also be stored, to enable computation of the confidence levels for other statistics.

The following paragraphs define the terms involved in the measurement process, spell out the measurement steps, and specify the data products.

5.1. Definitions

5.1.1. “Raw” Image and “Calibrated” Image. Standard techniques for the acquisition of CCD images are used. A “raw” image is the pixel-by-pixel image obtained by reading the charge from each pixel of the CCD, and amplifying and sending it to an analog-to-digital converter. A “calibrated” image is a raw image that has had background bias subtracted and the detector responsivity normalized by dividing by a flat-field image. (Saturated images are avoided in order to avoid the confusion of CCD blooming and other potential CCD nonlinearities.) A calibrated image can also include the step of low order aberration contribution subtraction based on wavefront information provided by a low order wavefront sensor (if implemented).

5.1.2. “Scratch” is a DM setting in which actuators are set to a predetermined surface figure that is approximately flat (typically, about 20 volts on each actuator).

5.1.3. The “algorithm” is the computer code that takes as input the measured speckle field images, and produces as output a voltage value to be applied to each element of the DM, with the goal of reducing the intensity of speckles.

5.1.4. The “star” is a small pinhole illuminated with laser or broadband light relayed via optical fiber from a source outside the CC vacuum wall (e.g., a laser or a filtered super-continuum white light source). The “small” pinhole is to be unresolved by the optical system; e.g., a 5- μm diameter pinhole would be “small” and unresolved by the 80- μm FWHM Airy disk in an f/100 beam at 600 nm wavelength. This “star” is the only source of light in the optical path of the CC. It is a stand-in for the star image that would have been formed by a telescope system.

5.1.5. The “contrast field” is a dimensionless map representing, for each detector pixel, the ratio of its value to the value of the peak of the PSF that would be measured in the same testbed conditions (light source, exposure time, Lyot stop, etc.) if the vortex mask were removed. The calibration of the contrast field is discussed in Section 5.3.

5.1.6. The “average contrast”, c_i , is a dimensionless quantity that is, for a given image, the spatial average value of the contrast field over the defined dark hole. Explicitly, an image’s average contrast is the sum of the contrast values for all pixels in the dark field, divided by the total number of pixels in the dark field, with no weighting applied.

5.1.7. The “mean contrast”, \hat{c} , of a given sequence of $n \geq 4$ images is the mean of the individual average contrast values occurring in that sequence:

$$\hat{c} = \frac{1}{n} \sum c_i.$$

5.1.8. “Milestone metric”. \hat{c} is the milestone metric.

5.1.9. “Standard Deviation”. The standard deviation σ_{meas} for an individual measurement of the average contrast value c_i is given as usual by:

$$\sigma_{meas} = \sqrt{\sum_{i=1}^n \frac{(c_i - \hat{c})^2}{n-1}}$$

The uncertainty in the mean contrast \hat{c} is then given by

$$\sigma_{mean} = \frac{\sigma_{meas}}{\sqrt{n}}.$$

There is also a contribution to the uncertainty from the independently-determined photometry error, σ_{phot} . The net standard deviation is thus

$$\sigma = \sqrt{\sigma_{mean}^2 + \sigma_{phot}^2}$$

5.1.10. “Statistical Confidence”. For contrast values that have a Gaussian distribution about the mean contrast, the statistical confidence that the mean contrast \hat{c} is less than some value c_0 is given by

$$conf(z < t) = \frac{1}{\sqrt{2\pi}} \int_{-\infty}^t e^{-z^2/2} dz = \frac{1}{2} + \frac{1}{\sqrt{2\pi}} \int_0^t e^{-z^2/2} dz$$

where $t = (c_0 - \hat{c})/\sigma$. Thus, as $\hat{c} = c_0 - t\sigma$, meeting a milestone contrast target c_0 with the desired confidence level requires the final measured mean contrast for a given run, \hat{c} , to be lower than the target contrast c_0 by t standard deviations. The Gaussian integral is widely tabulated, and $conf = 0.9$ implies $t = 1.28$. Thus, for 90% confidence, $\hat{c} = c_0 - 1.28\sigma$, i.e., the measured \hat{c} must be smaller than the target c_0 by 1.28σ .

5.2. Measurement of the Star Brightness

5.2.1. The vortex mask is displaced laterally relative to the center of the beam by approximately $10 \lambda/D$ or so, so as to transmit maximum stellar flux.

5.2.2. To create the photometric reference, a representative sample of short-exposure (e.g. a few milliseconds) images of the star is taken, with all coronagraph elements other than focal-plane vortex mask in place.

5.2.3. The images are averaged to produce a single star image. The “short-exposure peak value” of the star’s intensity is estimated. Since the star image is well-sampled in the CCD focal plane (the Airy disk is sampled by ~ 20 pixels within a radius equal to the full width half maximum), the star intensity can be estimated using either the value of the maximum-brightness pixel or an interpolated value representative of the apparent peak.

5.2.4. The “peak count rate” (counts/sec) is measured for exposure times of microseconds to tens of seconds.

5.3. Measurement of the Coronagraph Dark Hole Contrast Field

5.3.1. The vortex mask is centered on the star image.

5.3.2. An image (typical exposure times are \sim tens of seconds) is taken of the coronagraph field (the suppressed star and surrounding speckle field). The dimensions of the target dark hole area, as shown schematically in Figure 18, are as defined in Fig. 6: A D-shaped field extending from 3 to $8\lambda/D$, bounded by a straight line passing $3\lambda/D$ from the star at its closest point, and by a circle of radius $8\lambda/D$ centered on the star.

5.3.3. The image is normalized to the “star brightness” as defined in 5.2, using the fixed ratio between peak star brightness and the integrated light in a region of the speckle field outside the central DM-controlled area. I.e., dark-hole/star = dark-hole/speckle * speckle/star. For this purpose, any well-defined region of the outer speckle field can be used; the red region in Figure 18 (taken from TPF-C Milestone Report #1, Trauger et al. 2006) is only illustrative.

(In slightly more detail, to avoid saturation issues with the full-flux image case, there are usually three ratios involved: dark hole pixel/distant speckle field (both obtained with the vortex in); distant speckle field/inner point spread function [out to several Airy rings (about 200 pixels); both obtained with vortex out]; and inner point spread function/central point spread function pixel [both with vortex out]). In our previous TDEM work, we found the distant speckle field to be unchanged by the insertion or removal [by lateral translation] of the vortex, thus providing a robust calibration ladder. Other calibration ladders may also be possible.

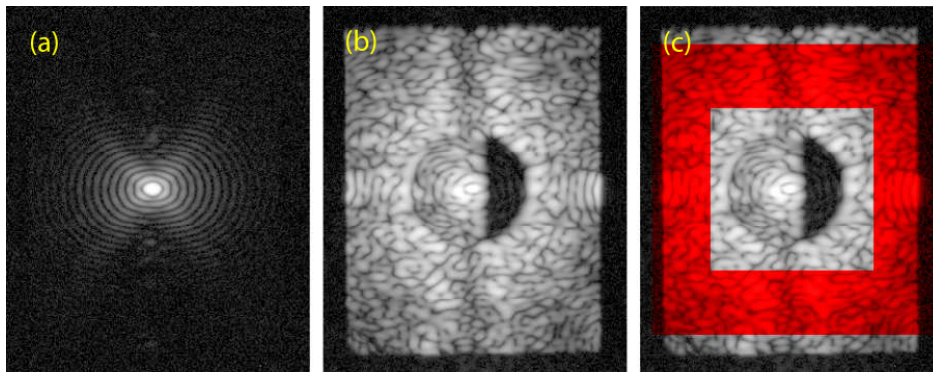


Figure 18. Reference field for contrast photometry. Shown here are (a) the “star” reference image, (b) the high-contrast coronagraph field; and (c) the same with a region of the reference speckle field in the “uncontrolled” area beyond the DM’s Nyquist limit superimposed in red. (Any subset of the red region can be used). Images are displayed with a logarithmic contrast stretch.

5.4. Milestone Demonstration Procedure

5.4.1. The DM is set to scratch. An initial coronagraph contrast field image is obtained as described in Sec. 5.3.

5.4.2. Wavefront sensing and control is performed to find settings of the DM actuators that give the required high-contrast in the target dark field. This iterative procedure may

take from one to several hours, starting from scratch, if no prior information is available. However it can take more or less time depending on the stability of the CC's optical system.

5.4.3. A number of contrast field images are taken, following steps 5.4.1 – 5.4.2. A sufficient number (≥ 4) of images are taken to provide statistical confidence that the milestone contrast levels have been achieved, as described in Section 5.1.

5.4.4. Laboratory data are archived for future reference, including all raw images of the reference star and contrast field images.

5.5. Milestone Data Package

The milestone certification data package will contain the following:

5.5.1. A narrative report that includes a discussion of how each element of the milestone was met, with a narrative summary of the overall milestone achievement and its repeatability.

5.5.2. A description of the optical elements, including the vortex masks, and their significant characteristics.

5.5.3. A tabulation of the significant operating parameters of the apparatus.

5.5.4. A contrast field image representative of the data set, with appropriate numerical contrast values indicated, with coordinate scales indicated in units of Airy distance (λD).

5.5.5. A description of the data reduction algorithms, in sufficient detail to guide an independent analysis of the delivered data.

5.5.6. Average and mean contrast values and standard deviations for the data used to satisfy the milestone requirements, including a pixel-by-pixel histogram of contrast values across the dark field.

5.5.7. For each image reported as part of the milestone demonstration, the average contrast within the area spanning 3-4 λ/D .

6. Success Criteria

The following are the required elements of the milestone demonstration. Each element includes a brief rationale.

6.1. Illumination is 10% bandwidth light in single or dual polarization at a wavelength in the range of 300 nm $< \lambda < 1000$ nm.

Rationale: This milestone is an initial demonstration of the feasibility of the approach at a wavelength in the science band of WFIRST/Exo-C/Habex/LUVOIR.

6.2. A mean contrast of 1×10^{-9} or smaller shall be achieved in a 3 to 8 λ/D dark zone, as defined in Fig. 6.

Rationale: This provides evidence that the high contrast field is sufficiently dark to be useful for searching planets, and to carry out initial tests at small angles.

6.3. Criterion 6.2 shall be met with a confidence of 90% or better. Sufficient data must be taken to justify this statistical confidence.

Rationale: Assuming the contrasts have a Gaussian distribution about the mean, this demonstrates a statistical confidence of 90% that the contrast goal has been met.

6.4. Elements 6.1 – 6.3 must be satisfied on 3 separate occasions with a reset of the wavefront control system software (DM set to scratch) between each demonstration.

Rationale: This provides evidence of the repeatability of the contrast demonstration.

The wavefront control system software reset between data sets ensures that the different data sets can be considered as independent and do not represent an unusually good configuration that cannot be reproduced. For each demonstration the DM will begin from a "scratch" setting. There is no time requirement for the demonstrations, other than the time required to meet the statistics stipulated in the success criteria. There is no required interval between demonstrations; subsequent demonstrations can begin as soon as prior demonstrations have ended. There is also no requirement to turn off power, open the vacuum tank, or delete data relevant for the calibration of the DM influence function.

7. Schedule

The CC is currently being used for a series of DM tests related to the WFIRST coronagraph DMs, and it will likely free up for other uses, including ours, by the start of FY17 (Oct. 1, 2016), and perhaps a month sooner. However, we will have access to the CC's relevant optical breadboard in the open air to begin installation and alignment work almost immediately. We anticipate sharing the CC, and so will have access to it 1/3 of the time, with a second 1/3 being assigned to John Trauger for other work, and the final 1/3 being unallocated and held in reserve. We thus expect to have access to the CC vacuum chamber for 4 months of the year, with a possibility of additional time if it is critically needed. Our basic plan is to work in fairly regular in-out cycles, consisting of several (2-4) months of preparatory work (consisting of implementing optical and software upgrades, purchasing improved masks, carrying out optical realignments, analyzing data, etc.) followed by roughly 2 months of in-tank time. However, we note that the CC differs significantly from the HCIT in having much shorter vacuum cycle times, making it much easier to reallocate time resources in shorter blocks to take ongoing developments or critical schedule needs into account. The exact dates of our in-out switches are thus expected to be much more flexible than the HCIT infrastructure allowed. The exact timing will thus be subject to ongoing coordination with the other tank occupant on a regular basis, so as to optimize both of our schedules.

Once the CC becomes available, this essentially brand new coronagraphic facility will need to be brought up to full functionality for the first time. We estimate that this first step will take approximately 6 months, followed by 4 months to demonstrate monochromatic contrasts with an old mask at the 10^{-9} level to demonstrate that we can operate as well as we did in the HCIT, 4 months to reach 10^{-8} contrast with 10% bandwidth, and a final 6 months to reach a contrast of 10^{-9} with 10% bandwidth, for a total of 20 months. The final 4 months will be devoted to writing up the milestone report and publishing results.

8. References

- Give'on, A., B. Kern, S. Shaklan, D. Moody, and L. Pueyo, "Broadband wavefront correction algorithm for high-contrast imaging systems," *Proc. SPIE* **6691**, 66910A, 2007.
- Guyon, O., Pluzhnik, E.A., Kuchner, M.J., Collins, B., and Ridgway, S.T. "Theoretical Limits On Extrasolar Terrestrial Planet Detection with Coronagraphs, *Ap.J. Suppl.* **167**, 81, 2006.
- Krist, J. et al., milestone report, 2012, in prep.
- Levine, M., Shaklan, S. & Kasting, J., "Terrestrial Planet Finder Coronagraph: Science and Technology Definition Team Report", JPL Publ. D-34923, 2006.
- Mawet, D., Riaud, P., Absil, O. and Surdej, J., "Annular Groove Phase Mask Coronagraph" *ApJ*, **633**, 1191, 2005.
- Mawet, D. Serabyn, E., Liewer, K., Hanot, Ch., McEldowney, S., Shemo, D. & O'Brien, N., "Optical Vectorial Vortex Coronagraphs using Liquid Crystal Polymers: Theory, Manufacturing and Laboratory Demonstration," *Optics Express*, **17**, 1902, 2009.
- Mawet, D. et al., "Taking the vector vortex coronagraph to the next level for ground- and space-based exoplanet imaging instruments: review of technology developments in the USA, Japan, and Europe," *Proc. SPIE* **8151**, 815108-1, 2011a.
- Mawet, D., et al. (2011b), "Recent Results of the Second Generation of Vector Vortex Coronagraphs on the High-contrast Imaging Testbed at JPL." *Proceedings of SPIE* **8151**, 81511D-8, 2011b.
- Serabyn E., D. Mawet & R. Burruss, "The potential of small space telescopes for exoplanet observations," E. Serabyn, *Proc. SPIE* **7731**, 77312O, 2010.
- Serabyn E., & Mawet, D. "Technology Development for Space Based Vortex Coronagraphy," *Proc. 2012 IEEE Aerospace Conf.*, Digital Object Identifier: [10.1109/AERO.2012.6187180](https://doi.org/10.1109/AERO.2012.6187180), 2012a.
- Serabyn, E. & Mawet, D., "Detecting Exoplanets with a Liquid-Crystal-Based Vortex Coronagraph," *Mol. Cryst. Liq. Cryst.*, **559**, 69, 2012b.
- Swartzlander, G., "The optical vortex coronagraph," *J. Opt. A.*, **11**, 1464, 2009.
- Trauger, J. et al., "TPF-C Milestone #1 Report," JPL Document D-35484, July 2006.
- Trauger, J. and W. Traub, "A laboratory demonstration of the capability to image an Earth-like extrasolar planet," *Nature* **446**, 771, 2007.
- Trauger, J., A. Give'on, B. Gordon, B. Kern, A. Kuhnert, D. Moody, A. Niessner, F. Shi, D. Wilson, and C. Burrows, "Laboratory demonstrations of high-contrast imaging for space coronagraphy," *Proc. SPIE* **6693**, 66930X, 2007.
- Trauger, J. et al., "ACCESS – A Concept Study for the Direct Imaging and Spectroscopy of Exoplanetary Systems," in *Pathways towards Habitable Planets, ASP Conf. Series* **430**, 375, 2010.